Author(s): Ranta, Mikaela & Hinkkanen, Marko & Luomi, Jorma

Title: Rotor parameter identification of saturated induction machines

Year: 2009

Version: Post print

Please cite the original version:

Ranta, Mikaela & Hinkkanen, Marko & Luomi, Jorma. 2009. Rotor parameter identification of saturated induction machines. IEEE Energy Conversion Congress and Exposition, 2009. ECCE 2009. 8. ISBN 978-1-4244-2893-9 (printed). DOI: 10.1109/ecce.2009.5316136.

Rotor Parameter Identification of Saturated Induction Machines

Mikaela Ranta, Marko Hinkkanen, and Jorma Luomi
Helsinki University of Technology, Department of Electrical Engineering
P.O. BOX 3000, FI-02015 TKK, Finland

***Abstract*—An induction machine model is proposed for the identification of rotor parameters using high-frequency signal injection. The model includes both the magnetic saturation caused by the fundamental-wave components and the frequency dependence encountered in the signal injection method. Both the skin effect in the rotor winding and the eddy current losses in the rotor core are taken into account. Sinusoidal signal injection is used at several frequencies, and the model parameters are fitted to the results. The rotor leakage inductance and the rotor resistance valid at low slip frequencies are also obtained from the model directly. Experimental results for a 45-kW machine are presented. It is shown that the model fits well to the measured data in various operating points, and the accuracy of the identified parameters is good.**

I. Introduction

The control of induction machine drives is based on a machine model. The parameters of the model can be identified either during the commissioning of the drive or in an adaptive manner as the drive is running. The traditional way of identifying the parameters is to use no-load and locked-rotor tests. In practice, locking the rotor is usually not possible, but a similar test can be performed by means of high-frequency signal injection both at standstill [1] and in any operating point [2]. Many other types of identification methods, for instance various observer-based techniques, have also been developed [3].

There are a few major difficulties when using an identification method based on high-frequency signal injection. Due to magnetic saturation, the impedance seen by the injected signal depends on the direction of the signal, giving rise to a saturation-induced saliency [4], [5]. Another difficulty arises due to the skin effect in the squirrel cage winding [1], [2]. The rotor resistance increases as a function of the injection frequency whereas the rotor leakage inductance decreases. Moreover, the effect of iron losses in the rotor core may become significant at high frequencies and cause inaccuracies in the identified parameters. The skin effect in the rotor conductors has been modeled by analytical functions based on a simple rotor slot shape [6]. Lumped-parameter networks could offer a more general approach for the modeling of the skin effect in the rotor conductors and the eddy currents in the iron core [7], [8], [9].

This paper proposes a time-domain model for the identification of the magnetically saturated rotor parameters. The goal is to compensate for the phenomena caused by the frequency of the signal injection method. The identification is based on an induction machine model, where the effects of magnetic saturation, skin effect, and eddy currents in the rotor core are taken into account. The total leakage inductance and the total resistance are identified using high-frequency signal injection [10], and the parameters of the model are fitted to the impedances obtained at several injection frequencies. Experimental results of a 45-kW induction machine are presented.

II. Induction Machine Model

Vectors will be denoted by boldface lowercase letters and matrices by boldface uppercase letters. The matrix transpose will be marked with the superscript T. The identity matrix, the orthogonal rotation matrix, and the zero matrix are

$$\mathbf{I} = \begin{bmatrix} 1 & 0 \\ 0 & 1 \end{bmatrix}, \quad \mathbf{J} = \begin{bmatrix} 0 & -1 \\ 1 & 0 \end{bmatrix}, \quad \mathbf{O} = \begin{bmatrix} 0 & 0 \\ 0 & 0 \end{bmatrix} \tag{1}$$

respectively. Real-valued space vectors will be used; for example, the stator-current vector is $\boldsymbol{i}_\mathrm{s} = [i_\mathrm{sd}, i_\mathrm{sq}]^\mathrm{T}$. The magnitude of the stator-current vector is $i_\mathrm{s} = ||\boldsymbol{i}_\mathrm{s}||$ and the magnitudes of other vectors are denoted similarly.

A. Saturable Dynamic Model

The dynamic model of an induction machine shown in Fig. 1 is considered. The model is depicted in general coordinates rotating at arbitrary angular speed ω_s. The electrical angular speed of the rotor is ω_m. The angular speed of coordinates with respect to the rotor is $\omega_\mathrm{r} = \omega_\mathrm{s} - \omega_\mathrm{m}$, corresponding to the slip angular frequency in the case of synchronous coordinates.

The stator-voltage vector is $\boldsymbol{u}_\mathrm{s}$, the rotor-voltage vector $\boldsymbol{u}_\mathrm{r}$ (equals zero in cage-induction machines), the rotor-current vector $\boldsymbol{i}_\mathrm{r}$, the stator-flux vector $\boldsymbol{\psi}_\mathrm{s}$, and the rotor-flux vector $\boldsymbol{\psi}_\mathrm{r}$. The stator resistance is R_s and the rotor resistance R_r. The magnetizing inductance is L_m and the stator leakage inductance $L_{\mathrm{s}\sigma}$. The rotor leakage inductance is divided into two parts, a constant inductance L_b and a saturable inductance L_a.

The part of the rotor leakage flux flowing across the rotor slots through the rotor conductors is strongly influenced by the skin effect as the frequency increases. The skin effect can be modeled using the resistance R_b in parallel to L_b. In machines with closed rotor slots, the flux part through the thin iron bridges at the air gap surface is heavily influenced by the magnetic saturation, which is modeled using the saturable inductance L_a. The magnetic saturation should also be modeled in machines with semi-closed rotor slots. The eddy-current

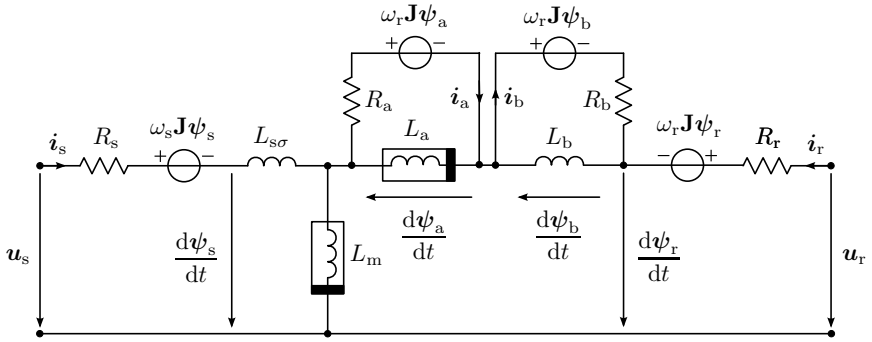

Fig. 1. Induction machine model in arbitrary reference frame, rotating at ω_s. The angular frequency $\omega_\mathrm{r} = \omega_\mathrm{s} - \omega_\mathrm{m}$, where ω_m is the angular speed of the rotor. The model takes into account the frequency-dependency in rotor parameters: the resistance R_a in parallel to L_a models the eddy currents in the saturable rotor core; the resistance R_b in parallel to L_b models the skin effect in the rotor conductors.

losses in the rotor core may have a relatively large influence at high signal injection frequencies, even though their influence on the fundamental-wave components is small. The iron losses are modeled by the resistance R_a in parallel to L_a. At zero frequency, the resistance of the rotor circuit corresponds to R_r, and the rotor leakage inductance corresponds to $L_\mathrm{a} + L_\mathrm{b}$.

The electrical dynamics of the induction machine, corresponding to Fig. 1, can be expressed as a nonlinear state-space representation,

$$\frac{\mathrm{d}\boldsymbol{\psi}}{\mathrm{d}t} = \boldsymbol{u} - \boldsymbol{R}\boldsymbol{i} - \boldsymbol{\Omega}\boldsymbol{\psi} \tag{2a}$$

$$\boldsymbol{i} = [\boldsymbol{L}(\boldsymbol{\psi})]^{-1}\boldsymbol{\psi} \tag{2b}$$

where the state vector, the input vector, and the output vector are

$$\boldsymbol{\psi} = \begin{bmatrix} \boldsymbol{\psi}_\mathrm{s} \\ \boldsymbol{\psi}_\mathrm{r} \\ \boldsymbol{\psi}_\mathrm{a} \\ \boldsymbol{\psi}_\mathrm{b} \end{bmatrix}, \quad \boldsymbol{u} = \begin{bmatrix} \boldsymbol{u}_\mathrm{s} \\ \boldsymbol{u}_\mathrm{r} \\ \mathbf{0} \\ \mathbf{0} \end{bmatrix}, \quad \boldsymbol{i} = \begin{bmatrix} \boldsymbol{i}_\mathrm{s} \\ \boldsymbol{i}_\mathrm{r} \\ \boldsymbol{i}_\mathrm{a} \\ \boldsymbol{i}_\mathrm{b} \end{bmatrix} \tag{3}$$

respectively. The resistance matrix and the back-emf matrix are

$$\boldsymbol{R} = \begin{bmatrix} R_\mathrm{s}\mathbf{I} & \mathbf{O} & \mathbf{O} & \mathbf{O} \\ \mathbf{O} & R_\mathrm{r}\mathbf{I} & \mathbf{O} & \mathbf{O} \\ \mathbf{O} & \mathbf{O} & R_\mathrm{a}\mathbf{I} & \mathbf{O} \\ \mathbf{O} & \mathbf{O} & \mathbf{O} & R_\mathrm{b}\mathbf{I} \end{bmatrix} \tag{4}$$

$$\boldsymbol{\Omega} = \begin{bmatrix} \omega_\mathrm{s}\mathbf{J} & \mathbf{O} & \mathbf{O} & \mathbf{O} \\ \mathbf{O} & \omega_\mathrm{r}\mathbf{J} & \mathbf{O} & \mathbf{O} \\ \mathbf{O} & \mathbf{O} & \omega_\mathrm{r}\mathbf{J} & \mathbf{O} \\ \mathbf{O} & \mathbf{O} & \mathbf{O} & \omega_\mathrm{r}\mathbf{J} \end{bmatrix} \tag{5}$$

respectively. The inductance matrix $\boldsymbol{L}(\boldsymbol{\psi})$ (or the nonlinear four-port inductor) determines the relationship between the currents and flux linkages. The inductance matrix can be expressed as

$$\boldsymbol{L} = \begin{bmatrix} L_\mathrm{s}\mathbf{I} & L_\mathrm{m}\mathbf{I} & \mathbf{O} & \mathbf{O} \\ L_\mathrm{m}\mathbf{I} & L_\mathrm{r}\mathbf{I} & L_\mathrm{a}\mathbf{I} & L_\mathrm{b}\mathbf{I} \\ \mathbf{O} & L_\mathrm{a}\mathbf{I} & L_\mathrm{a}\mathbf{I} & \mathbf{O} \\ \mathbf{O} & L_\mathrm{b}\mathbf{I} & \mathbf{O} & L_\mathrm{b}\mathbf{I} \end{bmatrix} \tag{6}$$

where the inductances may depend on the flux linkages. The stator inductance and the rotor inductance are defined by $L_\mathrm{s} = L_\mathrm{m} + L_{\mathrm{s}\sigma}$ and $L_\mathrm{r} = L_\mathrm{m} + L_\mathrm{a} + L_\mathrm{b}$, respectively. In the following, $L_{\mathrm{s}\sigma}$ is assumed constant for simplicity, but the magnetizing inductance is a function of the main flux $L_\mathrm{m} = L_\mathrm{m}(\psi_\mathrm{m})$ and the inductance L_a is a function of the flux $\boldsymbol{\psi}_\mathrm{a}$ $L_\mathrm{a} = L_\mathrm{a}(\psi_\mathrm{a})$. If needed, the saturation due to the main and leakage flux interaction could be included in the model [11].

B. Power Balance

For per-unit quantities, the power balance is obtained based on (2) as

$$\boldsymbol{i}_\mathrm{s}^\mathrm{T}\boldsymbol{u}_\mathrm{s} + \boldsymbol{i}_\mathrm{r}^\mathrm{T}\boldsymbol{u}_\mathrm{r} = R_\mathrm{s}i_\mathrm{s}^2 + R_\mathrm{r}i_\mathrm{r}^2 + R_\mathrm{a}i_\mathrm{a}^2 + R_\mathrm{b}i_\mathrm{b}^2 + \frac{\mathrm{d}W_\mathrm{f}}{\mathrm{d}t} + T_\mathrm{e}\omega_\mathrm{m} \tag{7}$$

where the electromagnetic torque is

$$T_\mathrm{e} = \boldsymbol{i}_\mathrm{s}^\mathrm{T}\mathbf{J}\boldsymbol{\psi}_\mathrm{s} \tag{8}$$

and the rate of change of the magnetic energy is

$$\begin{aligned} \frac{\mathrm{d}W_\mathrm{f}}{\mathrm{d}t} &= \boldsymbol{i}_\mathrm{s}^\mathrm{T}\frac{\mathrm{d}\boldsymbol{\psi}_\mathrm{s}}{\mathrm{d}t} + \boldsymbol{i}_\mathrm{r}^\mathrm{T}\frac{\mathrm{d}\boldsymbol{\psi}_\mathrm{r}}{\mathrm{d}t} + \boldsymbol{i}_\mathrm{a}^\mathrm{T}\frac{\mathrm{d}\boldsymbol{\psi}_\mathrm{a}}{\mathrm{d}t} + \boldsymbol{i}_\mathrm{b}^\mathrm{T}\frac{\mathrm{d}\boldsymbol{\psi}_\mathrm{b}}{\mathrm{d}t} \\ &= i_\mathrm{s}\frac{\mathrm{d}\psi_{\mathrm{s}\sigma}}{\mathrm{d}t} + i_\mathrm{m}\frac{\mathrm{d}\psi_\mathrm{m}}{\mathrm{d}t} + i_\mathrm{a}\frac{\mathrm{d}\psi_\mathrm{a}}{\mathrm{d}t} + i_\mathrm{b}\frac{\mathrm{d}\psi_\mathrm{b}}{\mathrm{d}t} \end{aligned} \tag{9}$$

The last form is obtained by assuming the flux vectors to be parallel with the corresponding current vectors in accordance with Fig. 1. If a flux-controlled (or current-controlled) inductor is lossless, it is reciprocal. The incremental inductance matrix associated with a reciprocal multi-port inductor is symmetric [12].

It is worth noticing that the steady-state losses in the resistors R_a and R_b can be expressed as

$$P_\mathrm{a} = \frac{\omega_\mathrm{r}^2\psi_\mathrm{a}^2}{R_\mathrm{a}}, \quad P_\mathrm{b} = \frac{\omega_\mathrm{r}^2\psi_\mathrm{b}^2}{R_\mathrm{b}} \tag{10}$$

respectively, for constant magnitude and constant angular frequency ω_r of the fluxes. These loss terms correspond to the eddy-current losses, i.e. they are proportional to the square of the flux amplitude and square of the frequency.

III. Linearized Small-Signal Model

In the following, tildes refer to the deviation about the operating point and operating-point quantities are marked with the subscript 0, e.g., $\tilde{\boldsymbol{u}}_\mathrm{s} = \boldsymbol{u}_\mathrm{s} - \boldsymbol{u}_\mathrm{s0}$. Synchronous coordinates rotating at constant angular speed ω_s0 are considered. The angular slip frequency is denoted by ω_r0.

A. Full-Order Small-Signal Model

The steady-state equations are obtained from (2) by substituting $\mathrm{d}/\mathrm{d}t = 0$:

$$\boldsymbol{u}_0 = \boldsymbol{R}[\boldsymbol{L}(\boldsymbol{\psi}_0)]^{-1}\boldsymbol{\psi}_0 + \boldsymbol{\Omega}\boldsymbol{\psi}_0 \tag{11a}$$

$$\boldsymbol{i}_0 = [\boldsymbol{L}(\boldsymbol{\psi}_0)]^{-1}\boldsymbol{\psi}_0 \tag{11b}$$

When solving the steady state, the order of the system can be reduced by assuming $\boldsymbol{i}_\mathrm{a0} = 0$ and $\boldsymbol{i}_\mathrm{b0} = 0$. This simplification leads to the conventional nonlinear T-equivalent circuit. An iterative method may be needed to solve the steady state, depending on the inductance functions in $\boldsymbol{L}(\boldsymbol{\psi})$.

The linearized small-signal model is given by

$$\frac{\mathrm{d}\tilde{\boldsymbol{\psi}}}{\mathrm{d}t} = \tilde{\boldsymbol{u}} - \boldsymbol{R}\tilde{\boldsymbol{i}} - \boldsymbol{\Omega}\tilde{\boldsymbol{\psi}} \tag{12a}$$

$$\tilde{\boldsymbol{i}} = \boldsymbol{L}_0^{-1}\tilde{\boldsymbol{\psi}} \tag{12b}$$

The inductance matrix of the linearized system is given in (13) at the bottom of the page. The incremental magnetizing inductance is denoted by L_mt0 and the incremental rotor leakage inductance is denoted by L_at0.

In the Laplace domain, the voltage deviation vector can be expressed as

$$\tilde{\boldsymbol{u}}(s) = \boldsymbol{Z}(s)\tilde{\boldsymbol{i}}(s) \tag{14}$$

where the impedance matrix is

$$\begin{aligned}\boldsymbol{Z}(s) &= s\boldsymbol{L}_0 + \boldsymbol{\Omega}\boldsymbol{L}_0 + \boldsymbol{R} \\ &= \begin{bmatrix} \boldsymbol{Z}_\mathrm{ss}(s) & \boldsymbol{Z}_\mathrm{sr}(s) & \mathbf{O} & \mathbf{O} \\ \boldsymbol{Z}_\mathrm{rs}(s) & \boldsymbol{Z}_\mathrm{rr}(s) & \boldsymbol{Z}_\mathrm{ra}(s) & \boldsymbol{Z}_\mathrm{rb}(s) \\ \mathbf{O} & \boldsymbol{Z}_\mathrm{ar}(s) & \boldsymbol{Z}_\mathrm{aa}(s) & \mathbf{O} \\ \mathbf{O} & \boldsymbol{Z}_\mathrm{br}(s) & \mathbf{O} & \boldsymbol{Z}_\mathrm{bb}(s) \end{bmatrix}\end{aligned} \tag{15}$$

The 2×2 submatrices in $\boldsymbol{Z}(s)$ can be evaluated using (4), (5), and (13).

In the following, $\tilde{\boldsymbol{u}}_\mathrm{r} = \mathbf{0}$ is assumed. The relationship between the stator voltage deviation and the stator current deviation is

$$\tilde{\boldsymbol{u}}_\mathrm{s}(s) = \boldsymbol{Z}_\mathrm{s}(s)\tilde{\boldsymbol{i}}_\mathrm{s}(s) \tag{16}$$

The 2×2 stator impedance matrix is

$$\boldsymbol{Z}_\mathrm{s}(s) = \boldsymbol{Z}_\mathrm{ss}(s) - \boldsymbol{Z}_\mathrm{sr}(s)\boldsymbol{Z}_\mathrm{x}^{-1}(s)\boldsymbol{Z}_\mathrm{rs}(s) \tag{17}$$

where

$$\begin{aligned}\boldsymbol{Z}_\mathrm{x}(s) = \boldsymbol{Z}_\mathrm{rr}(s) &- \boldsymbol{Z}_\mathrm{ra}(s)\boldsymbol{Z}_\mathrm{aa}^{-1}(s)\boldsymbol{Z}_\mathrm{ar}(s) \\ &- \boldsymbol{Z}_\mathrm{rb}(s)\boldsymbol{Z}_\mathrm{bb}^{-1}(s)\boldsymbol{Z}_\mathrm{br}(s)\end{aligned} \tag{18}$$

B. Reduced-Order Small-Signal Model

For the purpose of parameter identification, the full-order small-signal stator impedance (17) is too complicated. Therefore, a reduced-order model that can be applied at high frequencies is derived. A sinusoidal deviation having the angular frequency ω is considered.

At high frequencies, the current flows mostly through the rotor circuit and the influence of the magnetizing inductance is small. Thus, it is, reasonable to assume that the magnetizing inductance seen by the injected signal is not dependent on the direction of the signal. In other words, the second term in (13) is omitted. It should be noticed that the operating-point magnetizing inductance L_m0 varies as a function of the operating point due to the magnetic saturation. No restrictions are put on the variation of this inductance in the reduced-order small-signal model.

The injection frequency ω is much higher than the slip frequency, and it is assumed that the influence of the slip frequency on the small-signal model can be omitted. This assumption corresponds to $\omega_\mathrm{r0} = 0$ in (5).

Under the assumptions $L_\mathrm{mt0} = L_\mathrm{m0}$ and $\omega_\mathrm{r0} = 0$, the small-signal stator impedance (17) in the frequency domain becomes

$$\boldsymbol{Z}_\mathrm{s}(\mathrm{j}\omega) = \begin{bmatrix} Z_\mathrm{sdd} & Z_\mathrm{sdq} \\ Z_\mathrm{sqd} & Z_\mathrm{sqq} \end{bmatrix} = \mathrm{e}^{\vartheta_\mathrm{a0}\mathbf{J}} \begin{bmatrix} Z_\mathrm{dd} & Z_\mathrm{dq} \\ Z_\mathrm{qd} & Z_\mathrm{qq} \end{bmatrix} \mathrm{e}^{-\vartheta_\mathrm{a0}\mathbf{J}} \tag{19}$$

where ϑ_a0 is the angle of the operating-point rotor leakage flux $\boldsymbol{\psi}_\mathrm{a0}$. The matrix elements are given by

$$Z_\mathrm{dd} = R_\mathrm{s} + \mathrm{j}\omega L_{\mathrm{s}\sigma} + Z_\mathrm{mdd} \tag{20a}$$

$$Z_\mathrm{dq} = -\omega_\mathrm{s0} L_{\mathrm{s}\sigma} + \mathrm{j}\frac{\omega_\mathrm{s0}}{\omega} Z_\mathrm{mqq} \tag{20b}$$

$$Z_\mathrm{qq} = R_\mathrm{s} + \mathrm{j}\omega L_{\mathrm{s}\sigma} + Z_\mathrm{mqq} \tag{20c}$$

$$Z_\mathrm{qd} = \omega_\mathrm{s0} L_{\mathrm{s}\sigma} - \mathrm{j}\frac{\omega_\mathrm{s0}}{\omega} Z_\mathrm{mdd} \tag{20d}$$

$$\begin{aligned}\boldsymbol{L}_0 = &\begin{bmatrix} L_\mathrm{s0}\mathbf{I} & L_\mathrm{m0}\mathbf{I} & \mathbf{O} & \mathbf{O} \\ L_\mathrm{m0}\mathbf{I} & L_\mathrm{r0}\mathbf{I} & L_\mathrm{a0}\mathbf{I} & L_\mathrm{b}\mathbf{I} \\ \mathbf{O} & L_\mathrm{a0}\mathbf{I} & L_\mathrm{a0}\mathbf{I} & \mathbf{O} \\ \mathbf{O} & L_\mathrm{b}\mathbf{I} & \mathbf{O} & L_\mathrm{b}\mathbf{I} \end{bmatrix} \\ &+ \frac{L_\mathrm{mt0} - L_\mathrm{m0}}{\psi_\mathrm{m0}^2} \begin{bmatrix} \boldsymbol{\psi}_\mathrm{m0}\boldsymbol{\psi}_\mathrm{m0}^\mathrm{T} & \boldsymbol{\psi}_\mathrm{m0}\boldsymbol{\psi}_\mathrm{m0}^\mathrm{T} & \mathbf{O} & \mathbf{O} \\ \boldsymbol{\psi}_\mathrm{m0}\boldsymbol{\psi}_\mathrm{m0}^\mathrm{T} & \boldsymbol{\psi}_\mathrm{m0}\boldsymbol{\psi}_\mathrm{m0}^\mathrm{T} & \mathbf{O} & \mathbf{O} \\ \mathbf{O} & \mathbf{O} & \mathbf{O} & \mathbf{O} \\ \mathbf{O} & \mathbf{O} & \mathbf{O} & \mathbf{O} \end{bmatrix} + \frac{L_\mathrm{at0} - L_\mathrm{a0}}{\psi_\mathrm{a0}^2} \begin{bmatrix} \mathbf{O} & \mathbf{O} & \mathbf{O} & \mathbf{O} \\ \mathbf{O} & \boldsymbol{\psi}_\mathrm{a0}\boldsymbol{\psi}_\mathrm{a0}^\mathrm{T} & \boldsymbol{\psi}_\mathrm{a0}\boldsymbol{\psi}_\mathrm{a0}^\mathrm{T} & \mathbf{O} \\ \mathbf{O} & \boldsymbol{\psi}_\mathrm{a0}\boldsymbol{\psi}_\mathrm{a0}^\mathrm{T} & \boldsymbol{\psi}_\mathrm{a0}\boldsymbol{\psi}_\mathrm{a0}^\mathrm{T} & \mathbf{O} \\ \mathbf{O} & \mathbf{O} & \mathbf{O} & \mathbf{O} \end{bmatrix}\end{aligned} \tag{13}$$

where

$$Z_{\mathrm{mdd}} = \frac{\omega^2 L_{\mathrm{m0}}^2 R_{\mathrm{rdd}}}{\omega^2(L_{\mathrm{m0}}+L_{\mathrm{rdd}})^2+R_{\mathrm{rdd}}^2} + \mathrm{j}\omega\frac{L_{\mathrm{m0}}[R_{\mathrm{rdd}}^2+\omega L_{\mathrm{rdd}}(\omega L_{\mathrm{m0}}+\omega L_{\mathrm{rdd}})]}{\omega^2(L_{\mathrm{m0}}+L_{\mathrm{rdd}})^2+R_{\mathrm{rdd}}^2} \tag{21a}$$

$$Z_{\mathrm{mqq}} = \frac{\omega^2 L_{\mathrm{m0}}^2 R_{\mathrm{rqq}}}{\omega^2(L_{\mathrm{m0}}+L_{\mathrm{rqq}})^2+R_{\mathrm{rqq}}^2} + \mathrm{j}\omega\frac{L_{\mathrm{m0}}[R_{\mathrm{rqq}}^2+\omega L_{\mathrm{rqq}}(\omega L_{\mathrm{m0}}+\omega L_{\mathrm{rqq}})]}{\omega^2(L_{\mathrm{m0}}+L_{\mathrm{rqq}})^2+R_{\mathrm{rqq}}^2} \tag{21b}$$

The resistances are given by

$$R_{\mathrm{rdd}} = \frac{\omega^2 L_{\mathrm{at0}}^2 R_{\mathrm{a}}}{\omega^2 L_{\mathrm{at0}}^2+R_{\mathrm{a}}^2} + \frac{\omega^2 L_{\mathrm{b}}^2 R_{\mathrm{b}}}{\omega^2 L_{\mathrm{b}}^2+R_{\mathrm{b}}^2} + R_{\mathrm{r}} \tag{22a}$$

$$R_{\mathrm{rqq}} = \frac{\omega^2 L_{\mathrm{a0}}^2 R_{\mathrm{a}}}{\omega^2 L_{\mathrm{a0}}^2+R_{\mathrm{a}}^2} + \frac{\omega^2 L_{\mathrm{b}}^2 R_{\mathrm{b}}}{\omega^2 L_{\mathrm{b}}^2+R_{\mathrm{b}}^2} + R_{\mathrm{r}} \tag{22b}$$

and the inductances are

$$L_{\mathrm{rdd}} = \frac{L_{\mathrm{at0}} R_{\mathrm{a}}^2}{\omega^2 L_{\mathrm{at0}}^2+R_{\mathrm{a}}^2} + \frac{L_{\mathrm{b}} R_{\mathrm{b}}^2}{\omega^2 L_{\mathrm{b}}^2+R_{\mathrm{b}}^2} \tag{23a}$$

$$L_{\mathrm{rqq}} = \frac{L_{\mathrm{a0}} R_{\mathrm{a}}^2}{\omega^2 L_{\mathrm{a0}}^2+R_{\mathrm{a}}^2} + \frac{L_{\mathrm{b}} R_{\mathrm{b}}^2}{\omega^2 L_{\mathrm{b}}^2+R_{\mathrm{b}}^2} \tag{23b}$$

It can be seen that as the frequency ω increases, the inductances L_{rdd} and L_{rqq} decrease while the resistances R_{rdd} and R_{rqq} increase. The incremental inductance L_{at0} affects R_{rdd} and L_{rdd} while the operating-point inductance L_{a0} can be seen in R_{rqq} and L_{rqq}.

At high frequencies, the value of R_{rdd}^2 is much smaller than the values of $\omega^2 L_{\mathrm{m0}}^2$ and $\omega^2 L_{\mathrm{m0}} L_{\mathrm{rdd}}$. The impedances Z_{dd} and Z_{qq} can, therefore, be approximated as

$$Z_{\mathrm{dd}} = R_{\mathrm{s}} + \mathrm{j}\omega L_{\mathrm{s}\sigma} + \frac{L_{\mathrm{m0}}^2 R_{\mathrm{rdd}}}{(L_{\mathrm{m0}}+L_{\mathrm{rdd}})^2} + \mathrm{j}\omega\frac{L_{\mathrm{m0}} L_{\mathrm{rdd}}}{L_{\mathrm{m0}}+L_{\mathrm{rdd}}} \tag{24a}$$

$$Z_{\mathrm{qq}} = R_{\mathrm{s}} + \mathrm{j}\omega L_{\mathrm{s}\sigma} + \frac{L_{\mathrm{m0}}^2 R_{\mathrm{rqq}}}{(L_{\mathrm{m0}}+L_{\mathrm{rqq}})^2} + \mathrm{j}\omega\frac{L_{\mathrm{m0}} L_{\mathrm{rqq}}}{L_{\mathrm{m0}}+L_{\mathrm{rqq}}} \tag{24b}$$

The operating-point total resistance $R_{\sigma 0}$ and the total leakage inductance $L_{\sigma 0}$ can be evaluated at $\omega = 0$ from $\mathrm{Re}\{Z_{\mathrm{qq}}\}$ and $\mathrm{Im}\{Z_{\mathrm{qq}}\}/\omega$, respectively, resulting in

$$R_{\sigma 0} = R_{\mathrm{s}} + \frac{L_{\mathrm{m0}}^2}{(L_{\mathrm{m0}}+L_{\mathrm{a0}}+L_{\mathrm{b}})^2} R_{\mathrm{r}} \tag{25}$$

$$L_{\sigma 0} = L_{\mathrm{s}\sigma} + \frac{L_{\mathrm{m0}}}{L_{\mathrm{m0}}+L_{\mathrm{a0}}+L_{\mathrm{b}}}(L_{\mathrm{a0}}+L_{\mathrm{b}}) \tag{26}$$

IV. Parameter Identification

Due to the magnetic saturation, the machine appears to be salient, and the parameters obtained depend on the direction of the signal. This saliency can be seen in the stator impedance $\boldsymbol{Z}_{\mathrm{s}}$ as the element Z_{dd} differs from Z_{qq}. The operating-point inductance L_{a0} affects Z_{qq}, while Z_{dd} is affected by the incremental inductance L_{at0}. As the goal is to identify the operating-point parameters, Z_{qq} is the desired impedance element in the identification process. The influence of the skin effect on the measured impedance should be taken into account to obtain the operating-point parameters $R_{\sigma 0}$ and $L_{\sigma 0}$.

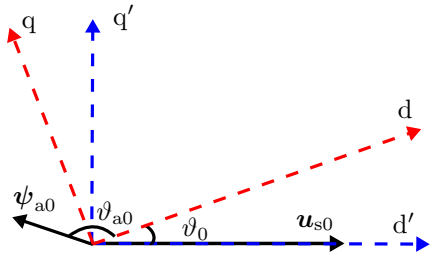

Fig. 2. The reference frames used in the identification.

In the following, a method for identifying the rotor parameters by means of high-frequency signal injection is proposed. In this approach, both the saturation-induced saliency and the skin effect are compensated. The stator impedance is measured in different directions to compensate the influence of the saturation and at several injection frequencies to compensate the influence of the skin effect and the eddy current losses.

A. Compensation of Saturation-Induced Saliency

In order to take into account the saturation-induced saliency, all elements in the impedance matrix $\boldsymbol{Z}_{\mathrm{s}}$ are measured. The impedance matrix can be obtained by injecting a voltage signal in two directions and measuring the components of the current response at the injection frequency. The signal is first injected parallel to the operating-point stator voltage and then perpendicular to the stator voltage. In this manner, all four elements $Z_{\mathrm{sdd}}, Z_{\mathrm{sdq}}, Z_{\mathrm{sqd}}$ and Z_{sqq} in the impedance matrix are obtained in a reference frame aligned with the operating-point stator voltage.

The impedance matrix can be evaluated in any reference frame by applying the coordinate transformation

$$\boldsymbol{Z}_{\mathrm{s}} = \mathrm{e}^{-\vartheta_0 \mathbf{J}} \boldsymbol{Z}_{\mathrm{s}}' \mathrm{e}^{\vartheta_0 \mathbf{J}} \tag{27}$$

where $\boldsymbol{Z}_{\mathrm{s}}'$ is the impedance matrix in the reference frame aligned with the operating-point stator voltage and ϑ_0 is the angle of the new reference frame in respect to the stator voltage. The reference frames and the angle ϑ_0 are illustrated in Fig. 2.

If the angle of the rotor leakage flux $\boldsymbol{\psi}_{\mathrm{a0}}$ would be known, the impedance could simply be evaluated in a reference frame aligned with $\boldsymbol{\psi}_{\mathrm{a0}}$. In (19), the angle ϑ_{a0} would be zero and the desired impedance $Z_{\mathrm{qq}} = Z_{\mathrm{sqq}}$.

As the rotor leakage flux angle is not known in practice, the impedance is evaluated as a function of the reference frame angle ϑ_0. As this angle varies, the angle ϑ_{a0} of the flux vector $\boldsymbol{\psi}_{\mathrm{a0}}$ in the reference frame considered also varies. According to (19)

$$\begin{aligned}\mathrm{Im}\{Z_{\mathrm{sqq}}\} = \mathrm{Im}\{Z_{\mathrm{qq}}\}\cos^2(\vartheta_{\mathrm{a0}}) + \mathrm{Im}\{Z_{\mathrm{dd}}\}\sin^2(\vartheta_{\mathrm{a0}}) \\ + \mathrm{Im}\{Z_{\mathrm{dq}}+Z_{\mathrm{qd}}\}\cos(\vartheta_{\mathrm{a0}})\sin(\vartheta_{\mathrm{a0}})\end{aligned} \tag{28}$$

The sum $\mathrm{Im}\{Z_{\mathrm{dq}}+Z_{\mathrm{qd}}\}$ is small compared to $\mathrm{Im}\{Z_{\mathrm{qq}}\}$ and $\mathrm{Im}\{Z_{\mathrm{dd}}\}$, and $\mathrm{Im}\{Z_{\mathrm{sqq}}\}$ varies sinusoidally between $\mathrm{Im}\{Z_{\mathrm{qq}}\}$ and $\mathrm{Im}\{Z_{\mathrm{dd}}\}$ as the direction of the d-axis of the reference frame varies. As the operating-point inductance L_{a0} is larger than the incremental inductance L_{at0}, the condition

$Z_{\rm qq} > Z_{\rm dd}$ holds. Hence, the maximum value of $\mathrm{Im}\{Z_{\rm sqq}\}$ should be chosen. The inductive part of the impedance can, thus, be obtained from

$$\mathrm{Im}\{Z_{\rm qq}\}/\omega = \max_{\vartheta_0}(\mathrm{Im}\{Z_{\rm sqq}(\vartheta_0)/\omega\}) \tag{29}$$

and in the same reference frame, the resistive part is obtained from

$$\mathrm{Re}\{Z_{\rm qq}\} = \mathrm{Re}\{Z_{\rm sqq}\} \tag{30}$$

B. Compensation of Skin Effect

The signal injection is repeated at several frequencies, and the impedance is obtained as a function of the frequency. To obtain the operating-point parameters, the cost function

$$J(L_{\rm a0}, L_{\rm b}, R_{\rm a}, R_{\rm b}) = \sum_{k=1}^{n}\Big(\mathrm{Re}\{\hat{Z}_{{\rm qq},k} - Z_{{\rm qq},k}\}\Big)^2 + \Big(\mathrm{Im}\{\hat{Z}_{{\rm qq},k} - Z_{{\rm qq},k}\}\Big)^2 \tag{31}$$

is minimized. $\hat{Z}_{\rm qq}$ is the estimated impedance calculated from (22b), (23b) and (24b), and $Z_{\rm qq}$ is the measured impedance. The inductance $L_{\rm a0}$ is saturable and depends on the operating point while the inductance $L_{\rm b}$ is constant. Therefore, the data fitting is based on data obtained from several operating points and several injection frequencies.

In addition to the fitting parameters $L_{\rm a0}, L_{\rm b}, R_{\rm a}$ and $R_{\rm b}$, the impedance $\hat{Z}_{\rm qq}$ is dependent on the stator resistance, the stator leakage inductance, the magnetizing inductance and the rotor resistance $R_{\rm r}$. The stator resistance is measured in advance by means of a DC test, and the stator flux is calculated as

$$\hat{\boldsymbol{\psi}}_{\rm s0} = -\mathbf{J}(\boldsymbol{u}_{\rm s0} - R_{\rm s}\boldsymbol{i}_{\rm s0})/\omega_{\rm s0} \tag{32}$$

The stator inductance can be obtained from [13]

$$\hat{L}_{\rm s0} = \frac{\hat{\psi}_{\rm s0}^2 - \hat{L}_{\sigma 0}\boldsymbol{i}_{\rm s0}^{\rm T}\hat{\boldsymbol{\psi}}_{\rm s0}}{\boldsymbol{i}_{\rm s0}^{\rm T}\hat{\boldsymbol{\psi}}_{\rm s0} - \hat{L}_{\sigma 0} i_{\rm s0}^2} \tag{33}$$

The total leakage inductance (26) can be substituted in (33), resulting in a second-order equation having the solutions

$$\hat{L}_{\rm s0} = \frac{-b \pm \sqrt{b^2 - 4ac}}{2a} \tag{34}$$

where

$$\begin{aligned} a &= \boldsymbol{i}_{\rm s0}^{\rm T}\hat{\boldsymbol{\psi}}_{\rm s0} - (L_{\rm s\sigma} + L_{\rm a0} + L_{\rm b})\boldsymbol{i}_{\rm s0}^{\rm T}\boldsymbol{i}_{\rm s0} \\ b &= 2(L_{\rm a0} + L_{\rm b})\boldsymbol{i}_{\rm s0}^{\rm T}\hat{\boldsymbol{\psi}}_{\rm s0} - \hat{\boldsymbol{\psi}}_{\rm s0}^{\rm T}\hat{\boldsymbol{\psi}}_{\rm s0} + L_{\rm s\sigma}^2\boldsymbol{i}_{\rm s0}^{\rm T}\boldsymbol{i}_{\rm s0} \\ c &= (L_{\rm s\sigma} - L_{\rm a0} - L_{\rm b})\hat{\boldsymbol{\psi}}_{\rm s0}^{\rm T}\hat{\boldsymbol{\psi}}_{\rm s0} - L_{\rm s\sigma}^2\boldsymbol{i}_{\rm s0}^{\rm T}\hat{\boldsymbol{\psi}}_{\rm s0} \end{aligned} \tag{35}$$

In the data fitting, the stator leakage inductance is assumed to be zero for simplicity. Thus, the parameters obtained in the identification correspond to the Γ-equivalent circuit [14], and the magnetizing inductance is obtained as $L_{\rm m0} = L_{\rm s0} - L_{\rm s\sigma} = L_{\rm s0}$. To avoid inconsistency with the operating-point data, the expressions

$$\hat{\boldsymbol{i}}_{\rm r0} = \hat{\boldsymbol{\psi}}_{\rm s0}/\hat{L}_{\rm m0} - \boldsymbol{i}_{\rm s0} \tag{36}$$

$$\hat{R}_{\rm r} = -\frac{\omega_{\rm r0}\hat{L}_{\rm m0}\hat{\boldsymbol{i}}_{\rm r0}^{\rm T}\mathbf{J}\boldsymbol{i}_{\rm s0}}{\hat{\boldsymbol{i}}_{\rm r0}^{\rm T}\hat{\boldsymbol{i}}_{\rm r0}} \tag{37}$$

are utilized to obtain the rotor resistance $\hat{R}_{\rm r}$.

TABLE I
ACTUAL PARAMETER VALUES IN SIMULATIONS

	Rated slip (p.u.)	10% of rated slip (p.u.)	No load (p.u.)
$L_{\rm a0}$	0.157	0.222	0.242
$L_{\rm b}$	0.107	0.107	0.107
$R_{\rm r}$	0.009	0.009	0.009
$R_{\rm a}$	7.46	7.46	7.46
$R_{\rm b}$	0.099	0.099	0.099

TABLE II
FITTED PARAMETER VALUES FROM SIMULATIONS

	Rated slip (p.u.)	10% of rated slip (p.u.)	No load (p.u.)
$L_{\rm a0}$	0.160	0.224	0.239
$L_{\rm b}$	0.107	0.107	0.107
$R_{\rm r}$	0.009	0.009	0.009
$R_{\rm a}$	6.59	6.59	6.59
$R_{\rm b}$	0.090	0.090	0.090

V. SIMULATION RESULTS

Simulations were carried out in the Matlab/Simulink environment using the data of a 45-kW four-pole induction motor with skewed and closed rotor slots. The rated voltage of the machine is 400 V, the rated current is 81 A, the rated speed is 1477 r/min, and the rated torque 291 Nm. The simulation model was implemented according to (2). The magnetizing inductance and the rotor leakage inductance were modeled as functions of the main flux and the rotor leakage flux, i.e. $L_{\rm m}(\psi_{\rm m}, \psi_{\rm a})$ and $L_{\rm a}(\psi_{\rm m}, \psi_{\rm a})$. The stator leakage inductance was set to zero.

The parameters were identified at the stator frequency 0.5 p.u. in three operating points; the slip frequency was equal to its rated value, 10% of the rated value and zero. The actual rotor parameter values in these operating points are shown in Table I. The inductance $L_{\rm a}$ is dependent on the operating point while the other parameters are not. A voltage signal was injected in two directions at four different frequencies between 60 Hz and 110 Hz. A data fitting algorithm based on differential evolution was applied to minimize the cost function (31). The impedance obtained from the signal injection as well as the fitted impedance are shown in Fig. 3 as a function of the frequency, and the fitted parameter values are shown in Table II.

It can be seen that the accuracy of the operating-point parameters $L_{\rm a0}$, $L_{\rm b}$ and $R_{\rm r}$ is very good in all operating points. For comparison, the parameters were also identified using rotating signal injection [2]. In this case, the saturation-induced saliency cannot be taken into account, but the skin effect can be compensated for in the same manner as described in Section IV-B. However, even if the skin effect is taken into account, the error in the identified operating-point rotor leakage inductance $L_{\rm a0} + L_{\rm b}$ is about 20% in all operating points.

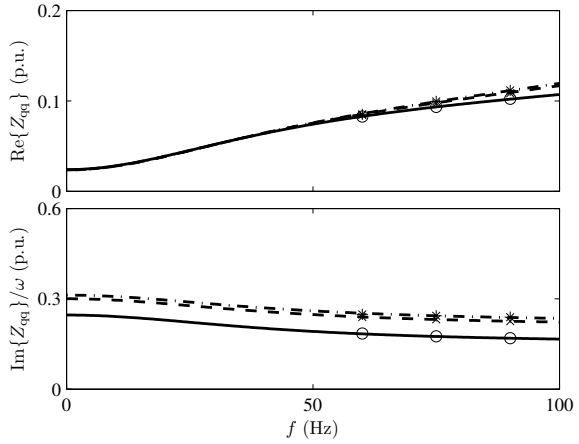

Fig. 3. Resistive part and inductive part of the impedance obtained from simulations of the 45-kW motor and fitted model as a function of the injection frequency f. The stator frequency is 0.5 p.u. The impedance obtained by signal injection is shown by circles at the rated slip frequency, by crosses at 10% of the rated slip frequency and by asterisks at no load. The corresponding fitted impedance is shown by solid lines, dashed lines and dash-dotted lines, respectively.

VI. Experimental Results

In the laboratory experiments, a four-pole 50-Hz 45-kW induction machine with skewed and closed rotor slots was fed by a frequency converter controlled by a dSpace DS1104 PPC/DSP board. The rating of the machine is the same as in the simulations. The load was controlled by a servo motor coupled to the shaft of the induction machine. The total moment of inertia of the setup is 0.81 kgm^2 (1.66 times the inertia of the rotor of the induction machine).

A. Compensation of Skin Effect at Standstill

The induction machine was magnetized with a DC-current vector at standstill. The parameters were measured at three different current levels; the stator current was 0 p.u., 0.3 p.u. (corresponding to the rated magnetizing current) and 0.4 p.u. The amplitude of the current signal was 0.15 p.u. In order to avoid speed variations, a current signal was injected only parallel to the DC-current vector. If the current signal were injected in a different direction, a nonzero torque would be produced. As the rotor is not locked, the torque would produce speed variations, which in turn would give cause to variations in the stator current. As a result, the impedance calculated from the stator voltage deviation and the stator current deviation would be incorrect. As the signal was injected in only one direction, it was possible to measure the impedance as a function of the frequency and to take the influence of the skin effect into account. However, the variation of the impedance as the direction of the excitation signal varies could not be taken into account.

At zero stator frequency, the stator flux cannot be calculated according to (32), and the stator (and magnetizing) inductance cannot be obtained from (33). Therefore, the influence of the magnetizing inductance on (24b) was omitted, i.e. $Z_{\mathrm{mqq}} \approx R_{\mathrm{rqq}} + \mathrm{j}\omega L_{\mathrm{rqq}}$. The rotor resistance R_{r} was allowed to vary freely in the data fitting. The fitted parameters are shown in Table III. In Fig. 4, the resistive and inductive parts of the measured impedance as well as the fitted results are shown as a function of the frequency.

TABLE III
Fitted Parameter Values at Standstill

	$i_{\mathrm{s0}} = 0.4$ p.u. (p.u.)	$i_{\mathrm{s0}} = 0.3$ p.u. (p.u.)	$i_{\mathrm{s0}} = 0$ p.u. (p.u.)
L_{a0}	0.240	0.282	0.367
L_{b}	0.084	0.084	0.084
R_{r}	0.012	0.012	0.012
R_{a}	5.51	5.51	5.51
R_{b}	0.027	0.027	0.027

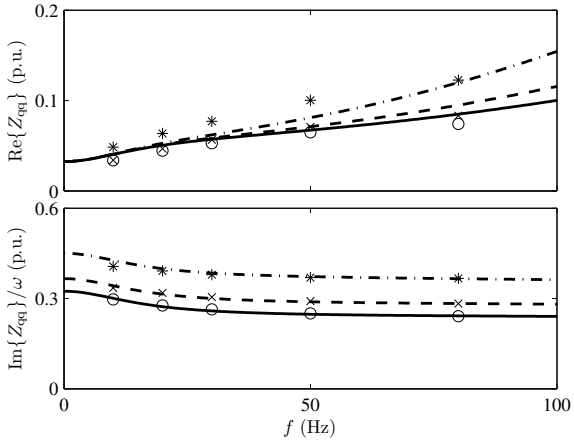

Fig. 4. Resistive and inductive part of the impedance obtained from measurements of the 45-kW motor and fitted model as a function of the injection frequency f when the motor is supplied by a DC voltage. The measured impedance is shown by circles as the stator current is 0.4 p.u., by crosses as the stator current is 0.3 p.u., and by asterisks as the current is zero. The corresponding fitted impedance is shown by solid lines, dashed lines and dash-dotted lines, respectively.

As the signal is injected only in one direction, the identification is easy to implement and the rotor does not have to be locked. Because of saturation due to the main flux and rotor leakage flux interaction [11], the inductance L_{a} decreases as the DC current increases as can be seen in Table III.

Due to the saturation, the impedance is dependent on the direction of the injection signal. This effect cannot be taken into account if the signal is injected in only one direction. When the signal is injected in the direction of the DC current, incremental parameters are obtained instead of operating-point parameters. The identification error is aggravated as the rotor leakage inductance not only saturates because of the stator current $\boldsymbol{i}_{\mathrm{s0}}$ but also because of the injection current. The magnetizing inductance is omitted in the data fitting, causing further errors in the identified parameters.

B. Proposed Method

The parameters were identified in three different operating points as the stator frequency was 0.5 p.u. The slip frequency

TABLE IV
FITTED PARAMETER VALUES AT HALF OF RATED SPEED

	Rated slip (p.u.)	10% of rated slip (p.u.)	No load (p.u.)
L_{a0}	0.148	0.251	0.554
L_{b}	0.107	0.107	0.107
R_{r}	0.010	0.010	0.010
R_{a}	7.46	7.46	7.46
R_{b}	0.099	0.099	0.099

was zero, 10% of the rated value, and equal to the rated value. A voltage signal was injected in two directions, and the influence of the magnetic saturation was taken into account as described in Section IV-A. Five frequencies between 60 Hz and 110 Hz were used for the signal injection. If lower frequencies are chosen, errors due to the variation in the rotor speed are easily encountered. The higher the injection frequency is, the smaller are the speed variations and their influence on the stator current. For the 45-kW machine, an injection frequency of 60 Hz is sufficient to keep the speed deviations small enough.

The fitted parameter values are given in Table IV. The resistive and inductive parts of the measured impedance and the fitted results are shown as a function of the signal frequency in Fig. 5. It can be seen that the model fits very well to the measured data. The rotor leakage inductance saturates at very low rotor currents, and the inductance is much larger in a no-load condition than when load is applied. Due to the high inductance L_{a0}, a larger part of the injection signal flows through the iron loss resistance R_{a} at no load than in the other operating points. Therefore, the resistive part of the impedance increases rapidly as a function of the frequency at no load. If the skin effect would not be taken into account, and the values measured at the frequency 60 Hz would be used, the error in the total leakage inductance could be as high as 28%, and the error in the total resistance could be even 460%.

As an example of the influence of the saturation, the measured parameters are shown as a function of the reference frame angle in Fig. 6 in the no-load case. The injection frequency is 60 Hz. If rotating signal injection would be used [2], approximately the mean value of the parameters would be obtained. The error caused by the saturation would then be about 16% in the inductance and 13% in the resistance at this injection frequency.

The influence of the saturation-induced saliency can also be seen by comparing the results at standstill to the results at half of the rated speed. The rated magnetizing current is 0.3 p.u. At the DC-current level 0.3 p.u. and in the no-load operation at half of the rated speed, the magnetizing current is approximately the same and the rotor current is zero. However, as the angle-dependency of the small-signal impedance is not taken into account at standstill, the value of the identified operating-point rotor leakage inductance ($L_{\mathrm{a0}} + L_{\mathrm{b}}$) is only 55% of the value obtained at half of the rated speed. The accuracy at standstill could be improved by measuring the entire impedance matrix, which would require the rotor to be locked.

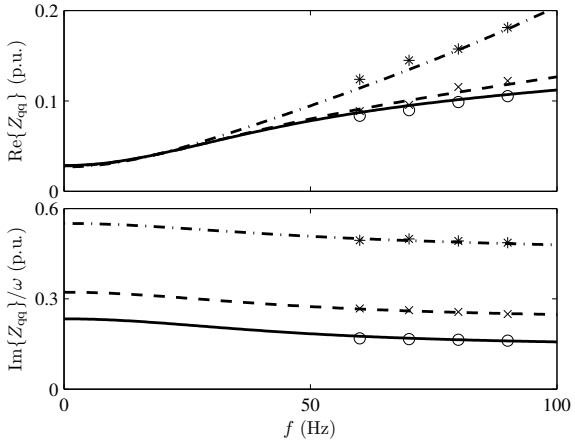

Fig. 5. Resistive part and inductive part of the impedance obtained from measurements of the 45-kW motor and fitted model as a function of the injection frequency f. The stator frequency is 0.5 p.u. The measured impedance is shown by circles at the rated slip frequency, by crosses at 10% of the rated slip frequency and by asterisks at no load. The corresponding fitted impedance is shown by solid lines, dashed lines and dash-dotted lines, respectively.

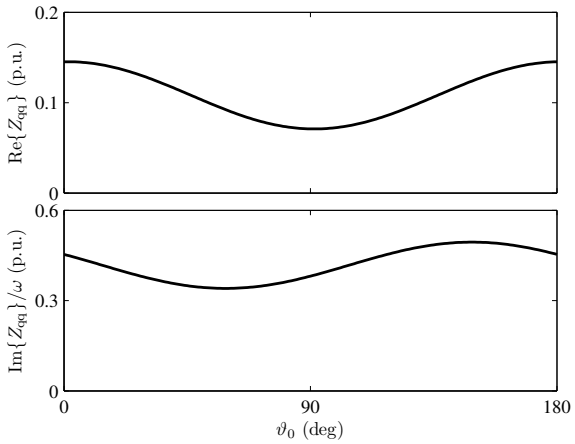

Fig. 6. Resistive part and inductive part of the measured impedance of the 45-kW motor as a function of the reference frame angle. The stator frequency is 25 Hz and the injection frequency is 60 Hz. No load is applied.

VII. CONCLUSIONS

When using high-frequency signal injection for the identification of the total leakage inductance and the total resistance of the induction machine, the saturation, the skin effect, and the iron losses should be taken into account. Due to the saturation, the small-signal impedance is dependent on the direction of the excitation signal. Because of the skin effect, the parameter values obtained at high frequencies deviate from the values at zero frequency. The iron losses might be relatively high at the injection frequencies, causing further inaccuracies in the identified parameters.

In this paper, the total leakage inductance and the total resistance are identified using sinusoidal signal injection. The

saturation-induced saliency is taken into account by evaluating the stator impedance in several reference frames. The impedance is measured at several frequencies, and a fitting algorithm is used to compensate for the skin effect and the eddy current losses. The model fits very well to the measured data, and the accuracy is significantly improved as compared to earlier methods.

REFERENCES

[1] R. J. Kerkman, J. D. Thunes, T. M. Rowan, and D. W. Schlegel, "A frequency-based determination of transient inductance and rotor resistance for field commissioning purposes," *IEEE Trans. Ind. Appl.*, vol. 32, no. 3, pp. 577–584, May/June 1996.

[2] D. Holliday, T. C. Green, and B. W. Williams, "On-line measurement of induction machine stator and rotor winding parameters," in *Proc. IEE PEVD Conf.*, London, U.K., Oct. 1994, pp. 485–469.

[3] H. A. Toliyat, E. Levi, and M. Raina, "A review of RFO induction motor parameter estimation techniques," *IEEE Trans. Energy Convers.*, vol. 18, no. 2, pp. 271–283, June 2003.

[4] V. Staudt, "Measuring differential inductances of asynchronous machines," *Euro. Trans. Electr. Power*, vol. 4, no. 1, pp. 27–33, Jan./Feb. 1994.

[5] M. L. Aime, M. W. Degner, and R. D. Lorenz, "Saturation measurements in AC machines using carrier signal injection," in *Conf. Rec. IEEE-IAS Annu. Meeting*, vol. 1, St. Louis, MO, Oct. 1998, pp. 159–166.

[6] Y.-S. Kwon, J.-H. Lee, S.-H. Moon, B.-K. Kwon, C.-H. Choi, and J.-K. Seok, "Standstill parameter identification of vector-controlled induction motor using frequency characteristics of rotor bars," in *Conf. Rec. IEEE-IAS Annu. Meeting*, Edmonton, Canada, Oct. 2008, CD-ROM.

[7] F. de Leon and A. Semlyen, "Time domain modeling of eddy current effects for transformer transients," *IEEE Trans. Power Delivery*, vol. 8, no. 1, pp. 271–280, Jan. 1993.

[8] J. L. Guardado, J. A. Flores, V. Venegas, J. L. Naredo, and F. A. Uribe, "A machine winding model for switching transient studies using network synthesis," *IEEE Trans. Energy Convers.*, vol. 20, no. 2, pp. 322–328, June 2005.

[9] E. Levi, A. Lamine, and A. Cavagnino, "Detuned operation of vector controlled induction machines due to stray load losses," in *Conf. Rec. IEEE-IAS Annu. Meeting*, vol. 1, Hong Kong, Oct. 2005, pp. 500–507.

[10] M. Ranta, M. Hinkkanen, and J. Luomi, "Inductance identification of and induction machine taking load-dependent saturation into account," in *Proc. ICEM'08*, Vilamoura, Portugal, Sept. 2008, CD-ROM.

[11] T. Tuovinen, M. Hinkkanen, and J. Luomi, "Modeling of mutual saturation in induction machines," in *Conf. Rec. IEEE-IAS Annu. Meeting*, Edmonton, Canada, Oct. 2008, CD-ROM.

[12] L. O. Chua, "Dynamic nonlinear networks: State-of-the-art," *IEEE Trans. Circuits Syst.*, vol. CAS-27, no. 11, pp. 1059–1087, Nov. 1980.

[13] J. L. Zamora and A. García-Cerrada, "Online estimation of the stator parameters in an induction motor using only voltage and current measurements," *IEEE Trans. Ind. Appl.*, vol. 36, no. 3, pp. 805–816, May/June 2000.

[14] G. R. Slemon, "Modelling of induction machines for electric drives," *IEEE Trans. Ind. Appl.*, vol. 25, no. 6, pp. 1126–1131, Nov./Dec. 1989.